# Disentangling the impact of the COVID-19 lockdowns on urban $NO_2$ from natural variability

Daniel L. Goldberg*[,1,3], Susan C. Anenberg[1], Debora Griffin[2], Chris A. McLinden[2], Zifeng Lu[3], David G. Streets[3]

[1]Department of Environmental and Occupational Health, George Washington University, Washington, DC, U.S.

[2]Air Quality Research Division, Environment and Climate Change Canada (ECCC), Toronto, Ontario, Canada

[3]Energy Systems Division, Argonne National Laboratory, Lemont, IL, U.S.

---

[*]Corresponding author. Phone: (202)994-8102; Email: dgoldberg@gwu.edu

## Abstract

Satellite data show substantial drops in nitrogen dioxide ($NO_2$) during COVID-19 physical distancing. To attribute $NO_2$ changes to $NO_X$ emissions changes over short timescales, one must account for meteorological effects. We find that meteorological patterns were especially favorable for low $NO_2$ in much of the U.S. in spring 2020, complicating comparisons with spring 2019. Meteorological variations between years can cause column $NO_2$ differences of ~15% over monthly timescales. After accounting for sun angle and meteorological considerations, we calculate that $NO_2$ drops ranged between 9.2 – 43.4% among twenty cities in North America, with a median of 21.6%. Of the studied cities, largest $NO_2$ drops (>30%) were in San Jose, Los Angeles, and Toronto, and smallest drops (<12%) were in Miami, Minneapolis, and Dallas. These normalized $NO_2$ changes can be used to highlight locations with greater activity changes and better understand the sources contributing to adverse air quality in each city.

## Plain-Language Summary

The current paradigm of disentangling emissions from meteorological influences on air pollution by averaging over many months has insufficient temporal granularity to quantify short-term emission changes. We developed two novel methods to account for weather impacts on daily pollution levels during COVID-19 precautions. Once we accounted for favorable weather conditions that in some cases kept air pollution low independent of tail-pipe emissions, calculated air pollutant emission reductions varied dramatically (9 – 43%) among twenty North American cities. Results can be used to understand factors contributing to inconsistent $NO_2$ changes during physical distancing, which can inform the effectiveness of COVID-19 protocols and aid future policy development. These methodologies will allow us to respond more quickly in future unintended experiments when emissions change suddenly.

## 1. Introduction

Nitrogen dioxide ($NO_2$) is unique due to its relatively short photochemical lifetime which varies from 2-6 h during the summer daytime (Beirle et al., 2011; de Foy et al., 2014; Laughner & Cohen, 2019; Valin et al., 2013) to 12-24 h during winter (Beirle et al., 2003; Shah et al., 2020). As a result, tropospheric $NO_2$ concentrations are strongly correlated with local $NO_X$ emissions, which are often anthropogenic in origin. However, due to the effects of meteorology and sun angle on the $NO_2$ abundance, $NO_2$ can vary by a factor of two simply due to seasonal changes (Pope et al., 2015; Wang et al., 2019). Therefore, satellite data are typically averaged over long timeframes (~seasonal/annual) to assess changes in $NO_X$ emissions (Duncan et al., 2016; Geddes et al., 2016; Georgoulias et al., 2019; Hilboll et al., 2013, 2017; Kim et al., 2009; Krotkov et al., 2016; Lamsal et al., 2015; McLinden et al., 2016; VanDerA et al., 2008).

With the COVID-19 crisis, there is now broad interest in rapid assessments of NOx emission changes on short timescales in locations that have implemented stay-at-home orders or other physical distancing measures. Using satellite data in this instance can be advantageous due to its global coverage at immediate timescales. However, current methods of averaging satellite $NO_2$ data over many months to minimize random daily effects of weather will not provide the temporal granularity needed to quantify short-lived $NO_X$ emission changes.

Preliminary satellite-based studies indicate that $NO_2$ dropped substantially in China following stringent COVID-19 physical distancing actions (F. Liu et al., 2020; Zhang et al., 2020). Similar declines have also been seen over northern Italy (ESA, 2020b) and India (ESA, 2020a). Although lockdown measures – and adherence to them – have been looser in the U.S. than in China, India, and Italy, preliminary analyses show that $NO_2$ amounts are declining across U.S. cities as well (NASA, 2020). These declines have, in some cases in the media (Holcombe & O'Key, 2020; Plumer & Popovich, 2020), been attributed to the emission changes during lockdowns, without accounting for the potentially substantial influences of meteorology and seasonality. Accounting for natural $NO_2$ fluctuations are especially important during spring, a time when the $NO_2$ concentrations and lifetimes are quickly changing due to transitioning meteorology, sun angle, and snow cover.

Understanding how NOx emissions have changed in response to physical distancing measures requires new methods to account for sun angle and meteorological conditions over very short time scales (days/weeks), as opposed to the traditional method of averaging over seasons and years. Here, we use three different methods to assess the $NO_2$ decreases associated with COVID-19 lockdowns. We combine TROPOMI $NO_2$ data with ERA5 re-analysis and a regional chemical transport model to determine the effects of the sun angle and meteorological factors – such as wind speed and wind direction – on $NO_2$ column amounts. The $NO_2$ changes after this "normalization" are more likely to represent the NOx emissions changes due to COVID-19.

## 2. Methods

### 2.1 TROPOMI $NO_2$

TROPOMI was launched by the European Space Agency (ESA) for the European Union's Copernicus Sentinel 5 Precursor (S5p) satellite mission on October 13, 2017. The satellite follows a sun-synchronous, low-earth (825 km) orbit with a daily equator overpass time of approximately 13:30 local solar time (VanGeffen et al., 2019). TROPOMI measures total column amounts of several trace gases in the Ultraviolet-Visible-Near Infrared-Shortwave Infrared spectral regions (Veefkind et al., 2012). At nadir, pixel sizes are $3.5 \times 7$ km$^2$ (reduced to $3.5 \times 5.6$ km$^2$ on August 6, 2019) with little variation in pixel sizes across the 2600 km swath.

Using a differential optical absorption spectroscopy (DOAS) technique on the radiance measurements in the 405 – 465 nm spectral window, the top-of-atmosphere spectral radiances can be converted into slant column amounts of $NO_2$ between the sensor and the Earth's surface (Boersma et al., 2018). In two additional steps, the slant column quantity can be converted into a tropospheric vertical column content, which is the quantity used most often to further our understanding of $NO_2$ in the atmosphere (Beirle et al., 2019; Dix et al., 2020; Goldberg et al., 2019; Griffin et al., 2019; Ialongo et al., 2020; Reuter et al., 2019; Zhao et al., 2020).

### 2.2 Meteorological Dataset

We use ERA5 meteorology((C3S), 2017) for the wind speed and direction in our analysis. When filtering the data based on wind, we use the average 100-m winds during 16 – 21 UTC, which approximately corresponds to the TROPOMI overpass time over North America. To downscale the ERA5 re-analysis, which is provided at $0.25° \times 0.25°$, we spatially interpolate daily averaged winds to $0.01° \times 0.01°$ using bilinear interpolation. Due to our dependence on $0.25° \times 0.25°$

meteorology, any microscale features (e.g., sea breezes) will not be accounted for, but these effects should be minor for our particular analysis.

### 2.3 Calculation of $NO_2$ Changes

We calculate the $NO_2$ changes using three different methods. In Method 1, we compare an average of March 15, 2020 – April 30, 2020 to the same timeframe of 2019; this year-over-year comparison is used most often in satellite studies quantifying long-term changes in $NO_X$ emissions. In Method 2, we develop a strategy to account for varying weather patterns without the use of a chemical transport model. In this method, we normalize each day's $NO_2$ observation to a day with "standard" meteorology – similar to standard temperature and pressure (STP) conditions in a laboratory setting. We do this by accounting for four different day-varying effects; these are sun angle, wind speed, wind direction, and day-of-week. In all cases, we normalize city-specific conditions to those that are climatological on April 15$^{th}$. Finally, in Method 3, we infer a TROPOMI $NO_2$ column amount under normal circumstances using the GEM-MACH regional chemical transport model, and then compare the actual TROPOMI columns to the theoretical columns. Methods 2 & 3, both account for year-varying meteorology, while Methods 1 does not. A detailed description of Methods 2 & 3 can be found in the Supplemental.

## 3. Results

### 3.1 Sun Angle & Meteorological Relationships

In the top row of Figure 1, we show 2019 $NO_2$ column densities during the low sun-angle "cold" season (January – March, October – December) and high sun-angle "warm" season (May – September) in the continental United States and southern Canada.

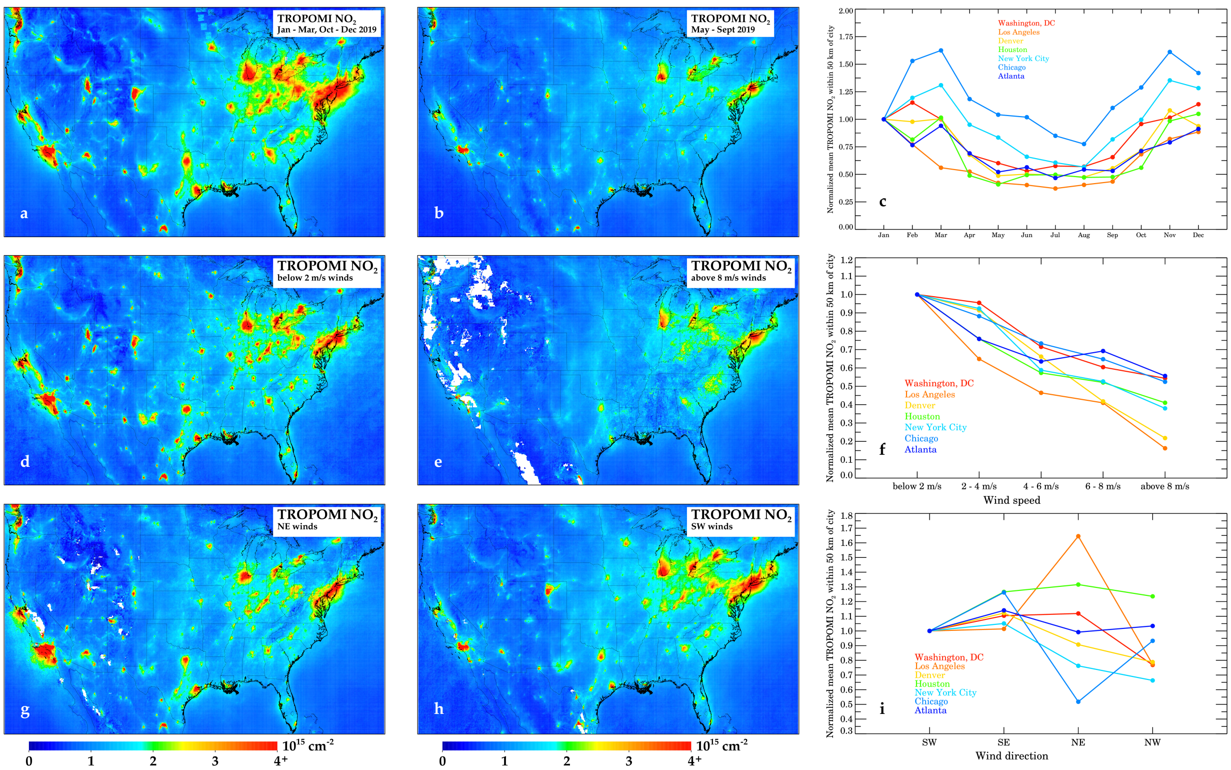


**Figure 1.** Effects of meteorology and sun angle on column $NO_2$. Top panels show (a) TROPOMI $NO_2$ during the warm season (May – Sept 2019), (b) during the cold season (Jan – Mar, Oct – Dec 2019), and (c) the monthly variation in 7 U.S. cities normalized to Jan 2019. Middle panels show (d) TROPOMI $NO_2$ when winds are < 2 m/s, (e) when winds are > 8 m/s, and (f) variations in $NO_2$ as a function of wind speed for seven cities normalized to stagnant conditions. Bottom panels show (g) TROPOMI $NO_2$ when winds are southwesterly, (h) when winds are northeasterly, and (i) variations as a function of wind direction for seven cities normalized to southwesterly winds.

Column $NO_2$ is larger during the cold season than during the warm season over the majority of our domain, despite $NO_X$ emissions generally peaking during the middle of the warm season due to a heavy air conditioning load (Abel et al., 2017; He et al., 2013). The larger $NO_2$ concentrations during the winter are instead due to the longer $NO_2$ lifetime during the cold season, primarily due to slower photolysis rates. When $NO_X$ is emitted during the warm season, it is transformed into other chemical species, such as $O_3$ and $HNO_3$, more quickly than during the winter. We find that in most near-urban locations column $NO_2$ amounts are 1.5 – 3 times larger during the winter than during the summer, and can vary substantially between city.

In a next step, we account for wind speed and wind direction in the spatiotemporal variation of $NO_2$ columns. In the middle and bottom panels of Figure 1, we demonstrate the effects of wind speed and wind direction on the $NO_2$ in our domain. Increases in wind speed yield $NO_2$ decreases due to quicker dispersion away from the city centers. For example, in New York City, Washington DC, Atlanta, and Chicago, all cities with relatively flat topography and located in the eastern United States, increasing wind speeds from nearly stagnant to > 8 m/s decreases $NO_2$ by 30 – 60%. Conversely, in Denver and Los Angeles, cities with more heterogeneous topography and with general isolation from an agglomeration of cities, show a stronger dependence on wind speed; increasing wind speeds from nearly stagnant to > 8 m/s decreases $NO_2$ by 70 – 85%. In both instances, these examples show the strong dependence of wind speed on local $NO_2$ amounts.

Similarly, wind direction has a large role in the local $NO_2$ amounts, although the effects of wind direction are non-linear. Generally, northwest winds yield the cleanest conditions in most U.S. cities, but the effects of other wind directions are more nuanced. For example, southwesterly winds yield the worst air quality in New York City, while northeasterly winds yield the largest $NO_2$ in Washington, D.C. This is due to the fact that the other city lies upwind in each opposing scenario. Changes in wind direction, given the same wind speed, can yield differences in $NO_2$ in major cities by up to 70%, and must be accounted for if properly attributing $NO_2$ changes to $NO_X$ emissions. Climatological patterns for all cities are shown in the Supplemental Material (Figures S1-S3).

While 2-m air temperature and boundary layer depth may be affecting the $NO_2$ concentrations, these are not independent of the aforementioned factors: sun angle, wind speed and wind direction. In fact, sun angle, wind speed, and wind direction are by themselves highly skilled predictors of near-surface temperatures and boundary layer depth in most instances. Since we are focused on mostly clear-sky days, clouds have limited effects here. Previous day's precipitation may also be a contributing factor to daily $NO_2$ amounts, but in many areas, the wind direction will partially account for this, since northwest winds usually follow large rain events in most areas.

### 3.2 Effects of COVID-19 physical distancing on $NO_2$

In order to quantify rapid changes in $NO_X$ due to COVID-19 physical distancing, we calculate $NO_2$ changes in North American cities using three different methods and a reference method. The results for all cities are shown in Table 1.

**Table 1.** Percentage drop in column $NO_2$ as observed by TROPOMI. Cities are listed by largest to smallest reduction as determined by the median of all three methods.

| | **Reference case** | **Account for sun-angle only** | **Account for sun-angle & meteorology** | | | |
|---|---|---|---|---|---|---|
| | **Method 0** | **Method 1** | **Method 2** | **Method 3** | | |
| **City Name** | **Δ between months 2020 only (Jan-Feb vs. Mar 15 - Apr 30)** | **Δ between years 2019 vs. 2020 (Mar 15 - Apr 30)** | **Using ERA5 analogs to account for meteorology 2019 vs. 2020 (Mar 15 - Apr 30)** | **Using GEM-MACH to infer NO2, 2020 only (Mar 15 - Apr 30)** | ***Mean of Methods 1-3*** | ***Median of Methods 1-3*** |
| San Jose | 65.2% | 43.4% | 40.7% | 43.5% | 42.5% | **43.4%** |
| Los Angeles | 66.1% | 32.6% | 32.5% | 38.6% | 34.6% | **32.6%** |
| Toronto | 60.4% | 31.0% | 17.0% | 42.0% | 30.0% | **31.0%** |
| Philadelphia | 50.3% | 36.6% | 30.7% | 22.1% | 29.8% | **30.7%** |
| Denver | 25.8% | 29.2% | 23.4% | 39.1% | 30.6% | **29.2%** |
| Atlanta | 39.6% | 35.2% | 27.4% | 20.2% | 27.6% | **27.4%** |
| Detroit | 35.5% | 29.9% | 22.8% | 15.6% | 22.8% | **22.8%** |
| Boston | 40.3% | 22.8% | 23.5% | 17.8% | 21.4% | **22.8%** |
| Washington DC | 42.9% | 31.4% | 21.2% | 6.7% | 19.8% | **21.2%** |
| Montreal | 12.5% | 3.3% | 20.9% | 30.2% | 18.1% | **20.9%** |
| New York City | 32.7% | 20.2% | 20.0% | 17.9% | 19.4% | **20.0%** |
| New Orleans | 41.7% | 13.5% | 19.6% | 22.5% | 18.5% | **19.6%** |
| Las Vegas | 66.7% | 9.5% | 18.4% | 42.0% | 23.3% | **18.4%** |
| Houston | 38.9% | 26.3% | 15.6% | 1.9% | 14.6% | **15.6%** |
| Chicago | 31.0% | 23.6% | 14.9% | 3.5% | 14.0% | **14.9%** |
| Phoenix | 43.9% | 12.8% | 14.8% | 35.4% | 21.0% | **14.8%** |
| Austin | 34.3% | 14.5% | 9.4% | 16.1% | 13.3% | **14.5%** |
| Dallas | 41.9% | 11.9% | 3.6% | 16.7% | 10.7% | **11.9%** |
| Miami | 27.9% | 16.1% | -1.6% | 11.0% | 8.5% | **11.0%** |
| Minneapolis | 0.1% | 14.3% | 9.2% | 8.1% | 10.5% | **9.2%** |
| | | | | | | |
| Mean of each method | 39.9% | 22.9% | 19.2% | 22.5% | 21.6% | **21.6%** |

The reference method, Method 0, compares the pre-lockdown and post-lockdown periods and represents the "true" $NO_2$ change; however, this method does not account for seasonal changes and, thus, is not considered in the medians/means.

In Method 1, we compare an average of March 15, 2020 – April 30, 2020 to the same timeframe of 2019. In Figure 2, we show difference and ratio plots between these two years (i.e., Method

1). The largest decreases in $NO_2$ are near the major cities in North America. We also find regional decreases in the eastern North America. Conversely, the central and northwestern United States have seen little change between years, which is likely due to the high fraction of $NO_2$ attributed to biogenic sources and long-range transport. We also observe substantial decreases near retired electricity generating units in the western U.S. (Storrow, 2019)

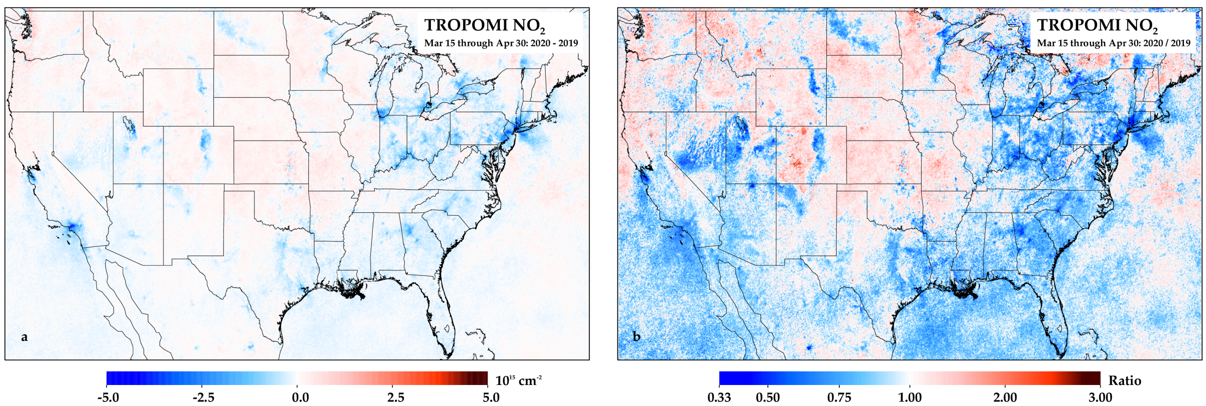


**Figure 2**. TROPOMI $NO_2$ differences between 2019 & 2020, using March 15 – April 30, 2020 as the post-COVID-19 period. Plots are showing (a) the absolute difference and (b) the ratio between years.

In Figure 3, we demonstrate Method 2. Here, we show the 2019 and 2020 28-day running TROPOMI $NO_2$ medians after accounting for sun angle and meteorology. In this figure, the January values are uniformly lower than their true values (Figure S4) because we are normalizing to April meteorological conditions (i.e., sun angle is higher in April as compared to January). In New York City, we calculate a 20.0% drop in $NO_2$ due to COVID-19 precautions. We find that there is no difference between Method 2 – which accounts for meteorology – and Method 1 – which only accounts for sun angle. This suggests that varying meteorological conditions in New York City, while different between years, may not have had a strong biasing effect. However, in Washington D.C. we find favorable conditions in 2020 as compared to 2019 because we observe substantially different $NO_2$ drops before (31.4%) and after (21.2%) correcting for the meteorology. These results are corroborated by the wind speed and direction (Figure S5). In 2019, winds were on average southwesterly, while in 2020, winds had more of a northwesterly and therefore cleaner component. Of all cities analyzed, we find that Miami had the most favorable conditions for low $NO_2$ in 2020 as compared to 2019; in 2020, winds were stronger from the south – in this case a cleaner air mass – than in 2019, which had relatively stagnant winds. Conversely, in Montreal, New Orleans, and Las Vegas, meteorological conditions appeared to be unfavorable in 2020 as compared to 2019.

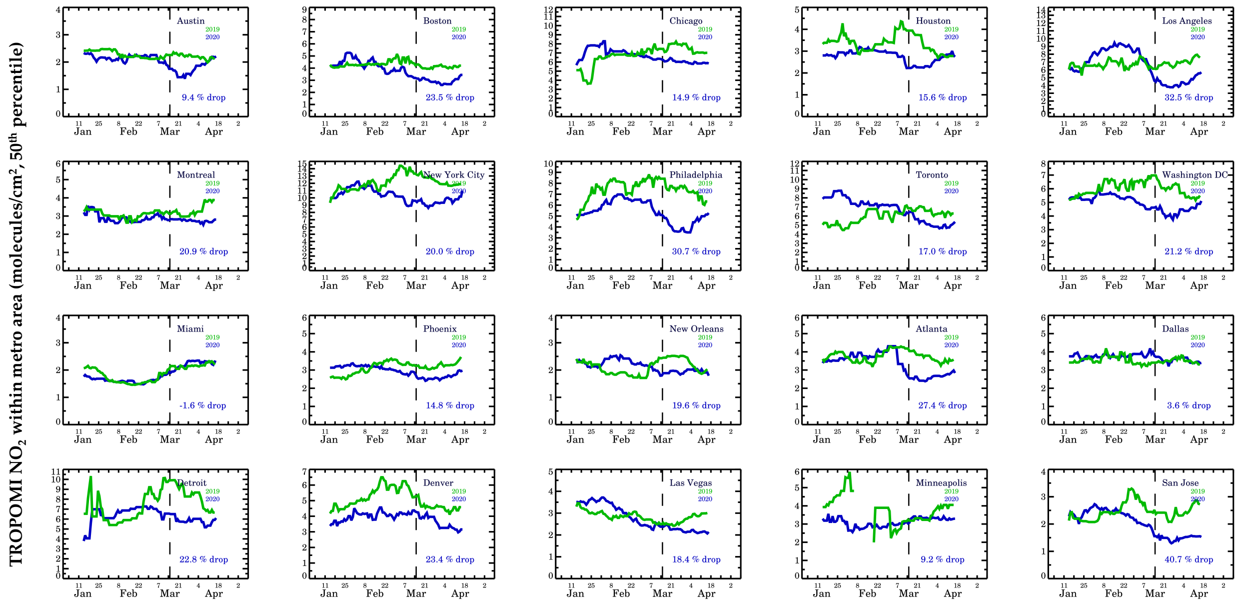

Time series (28-day rolling medians after normalizing for sun angle and meteorology)

**Figure 3**. Trends in TROPOMI $NO_2$ since January 1 in 2019 and 2020 after accounting for meteorological variability and sun angle. The lines represent the 28-day rolling median value (50$^{th}$ percentile) in a 0.4° × 0.4° box centered on the city center for the largest cities (New York City, Los Angeles, Chicago, Toronto, Houston) and 0.2° × 0.2° box in all other cities.

In Figure 4, we demonstrate Method 3, in which we account for meteorology and chemical interactions using a chemical transport model. We create a theoretical TROPOMI column $NO_2$ using ECCC's regional operational air quality forecast model (Moran et al., 2009; Pendlebury et al., 2018), which accounts for typical seasonal emission changes but not for any impacts due to the COVID-19 lockdowns; this helps provide expected $NO_2$ levels with a business as usual scenario. Around mid-March there is often a divergence between the expected and observed $NO_2$ in the major cities. Using this method, largest $NO_2$ reductions due to COVID-19 precautions are in Toronto, San Jose, and Las Vegas. Similar to Method 2, we find that $NO_2$ changes are generally smaller in the Northeastern U.S. and Florida as compared to Method 1 after accounting for meteorology. In fifteen of the twenty studied cities, we find that Methods 2 & 3, which utilize independent meteorological datasets, show similar biasing effects of meteorology (favorable vs. unfavorable) when compared to Method 1.

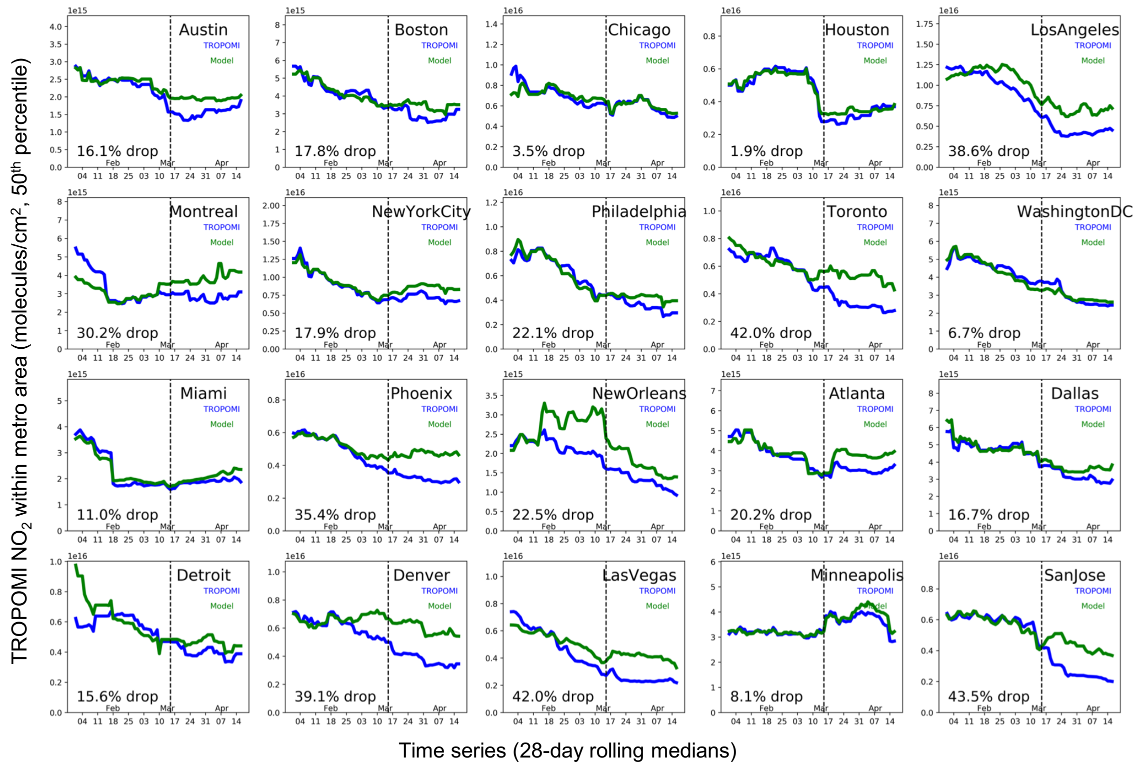


**Figure 4**. Trends in TROPOMI $NO_2$ since January 1, 2020. The actual observed columns are shown in black, while the "expected" columns - using GEM-MACH to infer $NO_2$ in the absence of lockdowns – is shown in blue. The lines represent the 28-day rolling median value (50$^{th}$ percentile) in a 0.4° × 0.4° box centered on the city center for the largest cities (New York City, Los Angeles, Chicago, Toronto, Houston) and 0.2° × 0.2° box in all other cities.

## 4. Discussion

Here we demonstrate two methodologies, Methods 2 & 3, to account for time-varying effects of meteorology on $NO_2$ concentrations. There are two main advantages for using Methods 2 & 3 to assess rapid changes in $NO_X$ as compared to a year-to-year comparison of the same month or seasonal period. Year-over-year technological improvements in the United States are generally causing $NO_X$ emissions to decrease over time, although we find a statistically insignificant $NO_2$ increase of 0.6% in our cities between 2019 and 2020 in the January – February average. Accounting for year-over-year changes would be more important if comparing 2020 values to years preceding 2019.

Perhaps more importantly, there are often different seasonal patterns between years, even when averaged over the entire season. Many longer-term meteorological patterns in North America can be attributed to the El Nino South Oscillation (ENSO) or the North Atlantic Oscillation

(NAO). In particular relevance to this analysis, the January – March 2019 period had a persistently negative NAO (https://www.cpc.ncep.noaa.gov/products/precip/CWlink/pna/month_nao_index.shtml) which allowed Arctic air to more readily intrude into the northern US than during more typical winters (https://www.ncdc.noaa.gov/sotc/national/201902). In January – March 2020, there was a consistently positive NAO which limited the influence of cold and relatively clean Arctic air in eastern North America, but instead yielded cloudier and wetter conditions. Similarly, ENSO can affect air quality in cities (Edwards et al., 2019; Shen & Mickley, 2017), but this had a minor effect between 2019 (Oceanic Niño Index: +0.8) and 2020 (Oceanic Niño Index: +0.5).

## 5. Conclusions

We estimate that $NO_X$ emissions temporarily dropped between 9 – 43% in North American cities due to COVID-19 precautions, with a median drop of 21.6% before and after COVID-19 physical distancing. If the sun angle is not accounted for, then the median $NO_2$ drop is 39.9%; this represents the true change of $NO_2$ in cities, but is not analogous to a change in $NO_X$ emissions. Our reported median drop of 21.6% is marginally lower than the 22.9% in a simple year-to-year comparison, which suggests that 2020 meteorology was slightly favorable for lower $NO_2$, although these effects are most pronounced in the Northeastern United States and Florida.

A deficiency of our method is our reliance on a single satellite instrument and algorithm. It is known that the operational TROPOMI $NO_2$ algorithm underestimates tropospheric vertical column $NO_2$ in urban areas due to its reliance on a global model to provide shape profiles for the air mass factor (AMF); investigating the effects of the AMF bias on trends will be the subject of future work. Also, there may be a clear-sky bias (Geddes et al., 2012) associated with TROPOMI retrievals, but the results presented here are generally consistent with studies using ground monitors over the coincident region (Bekbulat et al., 2020) and the reported $CO_2$ emissions reductions due to COVID-19 precautions (Le Quéré et al., 2020).

The estimates of $NO_2$ changes using our Methods appear to be reasonable given a quick bottom-up emissions calculation. Assuming that passenger vehicles traffic dropped by ~50%, and that all other sources only dropped modestly ~10 – 25%, $NO_X$ reductions between 10 – 35% would be expected. San Jose, Los Angeles and Toronto appear to have reductions at the high end of this range, while Miami, Minneapolis, and Dallas have values near the lowest end; further work will look into why these cities have reductions on the ends of the spectrum. Rapid assessments of $NO_2$ changes – after normalized for seasonal and meteorological factors – can be used to highlight locations with greater changes in activity and better understand the sources contributing to adverse air quality in each city.

**Acknowledgments**

This work has been supported by NASA through a Rapid Response grant, a Health and Air Quality (HAQ) grant (award #: 80NSSC19K0193), and two Atmospheric Composition Modeling and Analysis Program grants. The work has also been supported by the Department of Energy, Office of Fossil Energy. We would also like to acknowledge valuable comments during the manuscript preparation from Joanna Joiner and Lok Lamsal of NASA Goddard, Joel Dreessen of Maryland Department of the Environment, Lucas Henneman of Harvard University T.H. Chan School of Public Health, and A.R. "Ravi" Ravishankara of Colorado State University. TROPOMI $NO_2$ data can be freely downloaded from the European Space Agency Copernicus Open Access Hub or the NASA EarthData Portal (http://doi.org/10.5270/S5P-s4ljg54). ERA5 can be freely downloaded from the Copernicus Climate Change (C3S) climate data store (CDS) (https://cds.climate.copernicus.eu/#!/search?text=ERA5&type=dataset). The submitted manuscript has been created by UChicago Argonne, LLC, Operator of Argonne National Laboratory ("Argonne"). Argonne, a US Department of Energy Office of Science laboratory, is operated under contract no. DE-AC02-06CH11357.

**Author Contributions**

DLG drafted the concept, wrote the manuscript, and performed much of the analysis. SCA jointly drafted the concept and edited the manuscript. DG and CAM provided the regional chemical model data and related analysis, and edited the manuscript. ZL jointly drafted the concept, helped to process the TROPOMI $NO_2$ data, and edited the manuscript. DGS edited the manuscript.

## References


(C3S), C. C. C. S. (2017). ERA5: Fifth generation of ECMWF atmospheric reanalyses of the global climate. Retrieved May 1, 2020, from https://cds.climate.copernicus.eu/cdsapp#!/home

Abel, D. W., Holloway, T., Kladar, R. M., Meier, P., Ahl, D., Harkey, M., & Patz, J. (2017). Response of Power Plant Emissions to Ambient Temperature in the Eastern United States. *Environmental Science and Technology*, *51*(10), 5838–5846. https://doi.org/10.1021/acs.est.6b06201

Beirle, S., Platt, U., Wenig, M., & Wagner, T. (2003). Weekly cycle of NO2 by GOME measurements: A signature of anthropogenic sources. *Atmospheric Chemistry and Physics*, *3*(6), 2225–2232. https://doi.org/10.5194/acp-3-2225-2003

Beirle, S., Boersma, K. F., Platt, U., Lawrence, M. G., & Wagner, T. (2011). Megacity Emissions and Lifetimes of Nitrogen Oxides Probed from Space. *Science*, *333*(6050), 1737–1739. https://doi.org/10.1126/science.1207824

Beirle, S., Borger, C., Dörner, S., Li, A., Hu, Z., Liu, F., et al. (2019). Pinpointing nitrogen oxide emissions from space. *Science Advances*, *5*(11), eaax9800. https://doi.org/10.1126/sciadv.aax9800

Bekbulat, B., Apte, J. S., Millet, D. B., Robinson, A. L., Wells, K., & Marshall, J. D. (2020). PM 2.5 and ozone air pollution levels have not dropped consistently across the US followingsocietal covid response. https://doi.org/10.26434/CHEMRXIV.12275603

Boersma, K. F., Eskes, H. J., Richter, A., De Smedt, I., Lorente, A., Beirle, S., et al. (2018). Improving algorithms and uncertainty estimates for satellite NO2 retrievals: results from the quality assurance for the essential climate variables (QA4ECV) project. *Atmospheric Measurement Techniques*, *11*(12), 6651–6678. https://doi.org/10.5194/amt-11-6651-2018

Choi, S., Lamsal, L. N., Follette-Cook, M., Joiner, J., Krotkov, N. A., Swartz, W. H., et al. (2019). Assessment of NO2 observations during DISCOVER-AQ and KORUS-AQ field campaigns. *AMTD*. https://doi.org/10.5194/amt-2019-338

Dix, B., Bruin, J., Roosenbrand, E., Vlemmix, T., Francoeur, C., Gorchov-Negron, A., et al. (2020). Nitrogen Oxide Emissions from U.S. Oil and Gas Production: Recent Trends and Source Attribution. *Geophysical Research Letters*, *47*(1), 2019GL085866. https://doi.org/10.1029/2019GL085866

Duncan, B. N., Lamsal, L. N., Thompson, A. M., Yoshida, Y., Lu, Z., Streets, D. G., et al. (2016). A space-based, high-resolution view of notable changes in urban NOx pollution around the world (2005-2014). *Journal of Geophysical Research: Atmospheres*, *121*(2), 976–996. https://doi.org/10.1002/2015JD024121

Edwards, R. P., Engle, M., & Morris, G. (2019). Evaluation of El Niño-Southern oscillation influence on ozone exceedances along the United States Gulf Coast. *Atmospheric Environment*, 117127. https://doi.org/10.1016/j.atmosenv.2019.117127

ESA. (2020a). Air pollution drops in India following lockdown. Retrieved May 4, 2020, from http://www.esa.int/Applications/Observing_the_Earth/Copernicus/Sentinel-5P/Air_pollution_drops_in_India_following_lockdown

ESA. (2020b). Coronavirus: nitrogen dioxide emissions drop over Italy. Retrieved May 4, 2020, from http://www.esa.int/ESA_Multimedia/Videos/2020/03/Coronavirus_nitrogen_dioxide_emissions_drop_over_Italy

de Foy, B., Wilkins, J. L., Lu, Z., Streets, D. G., & Duncan, B. N. (2014). Model evaluation of methods for estimating surface emissions and chemical lifetimes from satellite data. *Atmospheric Environment*, *98*, 66–77. https://doi.org/10.1016/j.atmosenv.2014.08.051

Geddes, J. A., Murphy, J. G., O'Brien, J. M., & Celarier, E. A. (2012). Biases in long-term NO2 averages inferred from satellite observations due to cloud selection criteria. *Remote Sensing of Environment*, *124*(2), 210–216. https://doi.org/10.1016/j.rse.2012.05.008

Geddes, J. A., Martin, R. V., Boys, B. L., & van Donkelaar, A. (2016). Long-Term Trends Worldwide in Ambient NO 2 Concentrations Inferred from Satellite Observations. *Environmental Health Perspectives*, *124*(3), 281–289. https://doi.org/10.1289/ehp.1409567

van Geffen, J., Boersma, K. F., Eskes, H., Sneep, M., ter Linden, M., Zara, M., & Veefkind, J. P. (2020). S5P TROPOMI NO<sub>2</sub> slant column retrieval: method, stability, uncertainties and comparisons with OMI. *Atmospheric Measurement Techniques*, *13*(3), 1315–1335. https://doi.org/10.5194/amt-13-1315-2020

Georgoulias, A. K., van der A, R. J., Stammes, P., Boersma, K. F., & Eskes, H. J. (2019). Trends and trend reversal detection in 2 decades of tropospheric NO2 satellite observations. *Atmospheric Chemistry and Physics*, *19*(9), 6269–6294. https://doi.org/10.5194/acp-19-6269-2019

Goldberg, D. L., Lamsal, L. N., Loughner, C. P., Swartz, W. H., Lu, Z., & Streets, D. G. (2017). A high-resolution and observationally constrained OMI NO2 satellite retrieval. *Atmospheric Chemistry and Physics*, *17*(18), 11403–11421. https://doi.org/10.5194/acp-17-11403-2017

Goldberg, D. L., Lu, Z., Streets, D. G., de Foy, B., Griffin, D., McLinden, C. A., et al. (2019). Enhanced Capabilities of TROPOMI NO2 : Estimating NOx from North American Cities and Power Plants. *Environmental Science & Technology*, acs.est.9b04488. https://doi.org/10.1021/acs.est.9b04488

Griffin, D., Zhao, X., McLinden, C. A., Boersma, K. F., Bourassa, A., Dammers, E., et al. (2019). High-Resolution Mapping of Nitrogen Dioxide With TROPOMI: First Results and Validation Over the Canadian Oil Sands. *Geophysical Research Letters*, *46*(2), 1049–1060. https://doi.org/10.1029/2018GL081095

He, H., Hembeck, L., Hosley, K. M., Canty, T. P., Salawitch, R. J., & Dickerson, R. R. (2013). High ozone concentrations on hot days: The role of electric power demand and NOx emissions. *Geophysical Research Letters*, *40*(19), 5291–5294. https://doi.org/10.1002/grl.50967

Hilboll, A., Richter, A., & Burrows, J. P. (2013). Long-term changes of tropospheric NO2 over megacities derived from multiple satellite instruments. *Atmospheric Chemistry and Physics*, *13*(8), 4145–4169. https://doi.org/10.5194/acp-13-4145-2013

Hilboll, A., Richter, A., & Burrows, J. P. (2017). NO2 pollution over India observed from space - the impact of rapid economic growth, and a recent decline. *Atmospheric Chemistry and Physics Discussions*, *20*(2), 1–18. https://doi.org/10.5194/acp-2017-101

Holcombe, M., & O'Key, S. (2020). Satellite images show less pollution over the US as coronavirus shuts down public places. Retrieved from https://www.cnn.com/2020/03/23/health/us-pollution-satellite-coronavirus-scn-trnd/index.html

Ialongo, I., Virta, H., Eskes, H., Hovila, J., & Douros, J. (2020). Comparison of TROPOMI/Sentinel-5 Precursor NO2 observations with ground-based measurements in Helsinki. *Atmospheric Measurement Techniques*, *13*(1), 205–218. https://doi.org/10.5194/amt-13-205-2020

Kim, S. W., Heckel, A., Frost, G. J., Richter, A., Gleason, J., Burrows, J. P., et al. (2009). NO2 columns in the western United States observed from space and simulated by a regional chemistry model and their implications for NOx emissions. *Journal of Geophysical Research Atmospheres*, *114*(11), 1–29. https://doi.org/10.1029/2008JD011343

Kleipool, Q. L., Dobber, M. R., de Haan, J. F., & Levelt, P. F. (2008). Earth surface reflectance climatology from 3 years of OMI data. *Journal of Geophysical Research Atmospheres*, *113*(18), 1–22. https://doi.org/10.1029/2008JD010290

Krotkov, N. A., McLinden, C. A., Li, C., Lamsal, L. N., Celarier, E. A., Marchenko, S. V., et al. (2016). Aura OMI observations of regional SO2 and NO2 pollution changes from 2005 to 2015. *Atmospheric Chemistry and Physics*, *16*(7), 4605–4629. https://doi.org/10.5194/acp-16-4605-2016

Lamsal, L. N., Krotkov, N. A., Celarier, E. A., Swartz, W. H., Pickering, K. E., Bucsela, E. J., et al. (2014). Evaluation of OMI operational standard NO2 column retrievals using in situ and surface-based NO2 observations. *Atmospheric Chemistry and Physics*, *14*(21), 11587–11609. https://doi.org/10.5194/acp-14-11587-2014

Lamsal, L. N., Duncan, B. N., Yoshida, Y., Krotkov, N. A., Pickering, K. E., Streets, D. G., & Lu, Z. (2015). U.S. NO2 trends (2005-2013): EPA Air Quality System (AQS) data versus improved observations from the Ozone Monitoring Instrument (OMI). *Atmospheric Environment*, *110*(2), 130–143. https://doi.org/10.1016/j.atmosenv.2015.03.055

Laughner, J. L., & Cohen, R. C. (2019). Direct observation of changing NOx lifetime in North American cities. *Science*, *366*(6466), 723–727. https://doi.org/10.1126/science.aax6832

Laughner, J. L., Zare, A., & Cohen, R. C. (2016). Effects of daily meteorology on the interpretation of space-based remote sensing of NO2. *Atmospheric Chemistry and Physics*, *16*(23), 15247–15264. https://doi.org/10.5194/acp-16-15247-2016

Laughner, J. L., Zhu, Q., & Cohen, R. C. (2019). Evaluation of version 3.0B of the BEHR OMI NO2 product. *Atmospheric Measurement Techniques*, *12*(1), 129–146. https://doi.org/10.5194/amt-12-129-2019

Lin, J. T., Liu, M. Y., Xin, J. Y., Boersma, K. F., Spurr, R., Martin, R. V., & Zhang, Q. (2015).

Influence of aerosols and surface reflectance on satellite NO2 retrieval: Seasonal and spatial characteristics and implications for NOx emission constraints. *Atmospheric Chemistry and Physics*, *15*(19), 11217–11241. https://doi.org/10.5194/acp-15-11217-2015

Liu, F., Page, A., Strode, S. A., Yoshida, Y., Choi, S., Zheng, B., et al. (2020). Abrupt declines in tropospheric nitrogen dioxide over China after the outbreak of COVID-19. Retrieved from http://arxiv.org/abs/2004.06542

Liu, M., Lin, J., Boersma, K. F., Pinardi, G., Wang, Y., Chimot, J., et al. (2019). Improved aerosol correction for OMI tropospheric NO2 retrieval over East Asia: constraint from CALIOP aerosol vertical profile. *Atmospheric Measurement Techniques*, *12*(1), 1–21. https://doi.org/10.5194/amt-12-1-2019

Lorente, A., Folkert Boersma, K., Yu, H., Dörner, S., Hilboll, A., Richter, A., et al. (2017). Structural uncertainty in air mass factor calculation for NO2 and HCHO satellite retrievals. *Atmospheric Measurement Techniques*, *10*(3), 759–782. https://doi.org/10.5194/amt-10-759-2017

McLinden, C. A., Fioletov, V. E., Boersma, K. F., Kharol, S. K., Krotkov, N., Lamsal, L. N., et al. (2014). Improved satellite retrievals of NO2 and SO2 over the Canadian oil sands and comparisons with surface measurements. *Atmospheric Chemistry and Physics*, *14*(7), 3637–3656. https://doi.org/10.5194/acp-14-3637-2014

McLinden, C. A., Fioletov, V. E., Krotkov, N. A., Li, C., Boersma, K. F., & Adams, C. (2016). A Decade of Change in NO2 and SO2 over the Canadian Oil Sands As Seen from Space. *Environmental Science and Technology*, *50*(1), 331–337. https://doi.org/10.1021/acs.est.5b04985

Moran, M. D., Ménard, S., Talbot, D., Huang, P., Makar, P. A., Gong, W., et al. (2009). *Particulate-Matter Forecasting with GEM-MACH15, A New Canadian Air-Quality Forecast Model. In Air Pollution Modeling and Its Application XX*. Retrieved from http://www.nato.int/science

NASA. (2020). Pandemic Before and After: Northeast US 2015-2019 versus 2020. Retrieved from https://airquality.gsfc.nasa.gov/slider/northeast-2020

Palmer, P. I., Jacob, D. J., Chance, K., Martin, R. V., Spurr, R. J. D., Kurosu, T. P., et al. (2001). Air mass factor formulation for spectroscopic measurements from satellites: Application to formaldehyde retrievals from the Global Ozone Monitoring Experiment. *Journal of Geophysical Research: Atmospheres*, *106*(D13), 14539–14550. https://doi.org/10.1029/2000JD900772

Pendlebury, D., Gravel, S., Moran, M. D., & Lupu, A. (2018). Impact of chemical lateral boundary conditions in a regional air quality forecast model on surface ozone predictions during stratospheric intrusions. *Atmospheric Environment*, *174*, 148–170. https://doi.org/10.1016/j.atmosenv.2017.10.052

Plumer, B., & Popovich, N. (2020). Traffic and Pollution Plummet as U.S. Cities Shut Down for Coronavirus. Retrieved from https://www.nytimes.com/interactive/2020/03/22/climate/coronavirus-usa-traffic.html

Pope, R. J., Chipperfield, M. P., Savage, N. H., Ordóñez, C., Neal, L. S., Lee, L. A., et al. (2015). Evaluation of a regional air quality model using satellite column NO2: Treatment of observation errors and model boundary conditions and emissions. *Atmospheric Chemistry and Physics*, *15*(10), 5611–5626. https://doi.org/10.5194/acp-15-5611-2015

Le Quéré, C., Jackson, R. B., Jones, M. W., Smith, A. J. P., Abernethy, S., Andrew, R. M., et al. (2020). Temporary reduction in daily global CO2 emissions during the COVID-19 forced confinement. *Nature Climate Change*, 1–7. https://doi.org/10.1038/s41558-020-0797-x

Reuter, M., Buchwitz, M., Schneising, O., Krautwurst, S., O'Dell, C. W., Richter, A., et al. (2019). Towards monitoring localized CO2 emissions from space: co-located regional CO2 and NO2 enhancements observed by the OCO-2 and S5P satellit. *Atmospheric Chemistry and Physics Discussions*, 1–19. https://doi.org/10.5194/acp-2019-15

Russell, A. R., Perring, A. E., Valin, L. C., Bucsela, E. J., Browne, E. C., Wooldridge, P. J., & Cohen, R. C. (2011). A high spatial resolution retrieval of NO2 column densities from OMI: Method and evaluation. *Atmospheric Chemistry and Physics*, *11*(16), 8543–8554. https://doi.org/10.5194/acp-11-8543-2011

Shah, V., Jacob, D. J., Li, K., Silvern, R. F., Zhai, S., Liu, M., et al. (2020). Effect of changing NOx lifetime on the seasonality and long-term trends of satellite-observed tropospheric NO2 columns over China. *Atmospheric Chemistry and Physics Discussions*, *20*(3), 1483–1495. https://doi.org/10.5194/acp-2019-670

Shen, L., & Mickley, L. J. (2017). Effects of El Niño on Summertime Ozone Air Quality in the Eastern United States. *Geophysical Research Letters*, *44*(24), 12,543-12,550. https://doi.org/10.1002/2017GL076150

Storrow, B. (2019). America's mega-emitters are starting to close. Retrieved May 15, 2020, from https://www.eenews.net/stories/1060965553/

Valin, L. C., Russell, A. R., & Cohen, R. C. (2013). Variations of OH radical in an urban plume inferred from NO2 column measurements. *Geophysical Research Letters*, *40*(9), 1856–1860. https://doi.org/10.1002/grl.50267

VanDerA, R. J., Eskes, H. J., Boersma, K. F., van Noije, T. P. C., Van Roozendael, M., De Smedt, I., et al. (2008). Trends, seasonal variability and dominant NOx source derived from a ten year record of NO2 measured from space. *Journal of Geophysical Research Atmospheres*, *113*(4), 1–12. https://doi.org/10.1029/2007JD009021

VanGeffen, J. H. G. M., Eskes, H. J., Boersma, K. F., Maasakkers, J. D., & Veefkind, J. P. (2019). *TROPOMI ATBD of the total and tropospheric NO2 data products*. Retrieved from http://www.tropomi.eu/sites/default/files/files/publicS5P-KNMI-L2-0005-RP-ATBD_NO2_data_products-20190206_v140.pdf

Veefkind, J. P., Aben, I., McMullan, K., Förster, H., de Vries, J., Otter, G., et al. (2012). TROPOMI on the ESA Sentinel-5 Precursor: A GMES mission for global observations of the atmospheric composition for climate, air quality and ozone layer applications. *Remote Sensing of Environment*, *120*(2012), 70–83. https://doi.org/10.1016/j.rse.2011.09.027

Wang, C., Wang, T., & Wang, P. (2019). The Spatial–Temporal Variation of Tropospheric NO2 over China during 2005 to 2018. *Atmosphere*, *10*(8), 444. https://doi.org/10.3390/atmos10080444

Williams, J. E., Folkert Boersma, K., Le Sager, P., & Verstraeten, W. W. (2017). The high-resolution version of TM5-MP for optimized satellite retrievals: Description and validation. *Geoscientific Model Development*, *10*(2), 721–750. https://doi.org/10.5194/gmd-10-721-2017

Zhang, R., Zhang, Y., Lin, H., Feng, X., Fu, T.-M., & Wang, Y. (2020). NOx Emission Reduction and Recovery during COVID-19 in East China. *Atmosphere*, *11*(4), 433. https://doi.org/10.3390/atmos11040433

Zhao, X., Griffin, D., Fioletov, V., McLinden, C. A., Cede, A., Tiefengraber, M., et al. (2020). Assessment of the quality of TROPOMI high-spatial-resolution NO2 data products in the Greater Toronto Area. *Atmospheric Measurement Techniques*, *13*(4), 2131–2159. https://doi.org/10.5194/amt-13-2131-2020